HEFAT2008
6th International Conference on Heat Transfer, Fluid Mechanics and Thermodynamics
30 June to 2 July 2008
Pretoria, South Africa
Paper number: CE1

THERMO FLUID DYNAMIC EULER-LAGRANGE CFD ANALYSIS APPLIED TO WET FLUE GAS DESULPHURISATION TECHNOLOGY

Colombo E., Inzoli F., Marocco* L.
*Author for correspondence
Energy Department,
Politecnico di Milano,
Piazza Leonardo da Vinci, 32
20133, Milan, Italy
E-mail: luca.marocco@polimi.it

ABSTRACT

Wet Flue Gas Desulphurisation (FGD) technology is the most frequently used scrubbing process for sulphur dioxide (SO_2) reduction from coal-fired utility boilers. Wet limestone FGD-plants using Open Spray Tower (OST) technology are the most commonly used.

CFD has been used to investigate the gas-liquid fluid dynamics inside a counter-current OST and the heat transfer between the phases. The continuous phase (gas) is modelled in the Eulerian framework while the discrete phase (liquid droplets) in the Lagrangian frame of reference. Simulation results show good agreement with measurements on a pilot plant flue gas cleaning unit. The commercial code Fluent 6.3.26, completed with the necessary subroutines for liquid phase properties and slurry wall interaction, has been used for the calculations.

INTRODUCTION

Since power generation generally represents the largest single, controllable source of sulfur dioxide emissions, the industry has been especially challenged by environmental initiatives. Emission controls on modern power stations account for as much as 10–20% of the capital investment and constitute a significant operating and maintenance (O&M) expense.

The dominating flue gas desulphurization technology is based on absorption of SO_2 in a limestone slurry. The most commonly used scrubbing system is the counter current OST. Flue gas enters at the bottom and liquid is injected through nozzles, positioned at different levels in the tower. Each spray level consists of tangential-inlet, hollow cone or full cone spray nozzles.

In order to avoid flue gas by-pass effects, which reduce sulphur removal efficiency, it is desirable to obtain an equal distribution of flue gas velocity and slurry spray density at each scrubber cross section. This can be achieved through a correct configuration of the nozzles position at each spray level.

NOMENCLATURE

A	[m²]	Droplet surface area
Bi	[-]	Biot number
c_d	[kJ/kgK]	Specific heat of droplet
d_{drop}	[m]	Droplet diameter
D_{H_2O-air}	[m²/s]	Air-water binary mass diffusion coefficient
h	[W/m²K]	Convective heat transfer coefficient
h_{lv}	[kJ/kg]	Water latent heat of evaporation
h_s	[kJ/kg]	Enthalpy per unit mass at droplet surface
i	[kJ/kg]	Internal energy per unit mass
k	[m²/s²]	Turbulent kinetic energy
k_c	[W/mK]	Gas phase thermal conductivity
k_g	[m/s]	Gas-side mass transfer coefficient
m_d	[kg]	Droplet mass
n_i	[mol]	Mole number of species i
$P_{sat,H2O}$	[Pa]	Water saturation pressure
Pr	[-]	Prandtl number
$\dot{Q}$	[W]	Heat transfer rate to a droplet
$\Re$	[J/molK]	Universal gas constant
T_d	[K]	Droplet temperature
$\boldsymbol{u}$	[m/s]	Gas phase velocity vector
$\boldsymbol{v}$	[m/s]	Droplet absolute velocity vector
$\boldsymbol{v}_{norm}$	[m/s]	Vector of droplet velocity normal to the wall
$\boldsymbol{We}$	[-]	Weber number

Special characters

μ	[Ns/m²]	Flue gas laminar viscosity
μ_d	[Ns/m²]	Droplet laminar viscosity
μ_t	[Ns/m²]	Turbulent viscosity
ν	[m²/s]	Flue gas kinematic viscosity
ρ	[kg/m³]	Flue gas density
ρ_d	[kg/m³]	Droplet density
ρ_s	[kg/m³]	Suspended solids density
ω_A	[-]	Mass fraction of component A

Today the design of WFGD equipment is based on empirical and/or semi-empirical correlations between the most important process parameters. These expressions can only be used when the design parameters are inside the validity range of the correlated values. Extrapolation outside this range can lead to unexpected results that can compromise the operation of the entire WFGD plant. A 3-D model approach that describes the physics of the multiphase flow can be very helpful for new design configurations.

The CFD package FLUENT 6.3.26 has been used to simulate the gas-liquid flow and the gas to liquid heat transfer inside an OST. The continuous phase (flue gas) is modeled in the Eulerian framework while the discrete phase (liquid droplets) in the Lagrangian frame of reference. Momentum, energy and mass coupling between phases, and its impact on both the discrete phase trajectories and the continuous phase flow, has been included.

The numerical results are compared with experimental data from a pilot plant counter-current OST.

EULERIAN FRAMEWORK – FLUE GAS

Dispersed phase flows are flows in which one phase, the dispersed phase, is not materially connected.

Unlike the flow of a single phase gas, the carrier phase of a dispersed phase flow contains dispersed particles or droplets. The ideal situation would be to solve the governing conservation equations (continuity, momentum and energy) for the carrier phase by accounting for the boundary conditions imposed by each and every particle or droplet in the field., which would provide a complete description of the carrier phase throughout the mixture. Computationally this would require a grid dimension at least as small as the smallest particle in the field. Such a solution is beyond current computer capabilities. Therefore one must resort to the use of equations based on the average properties in the flow.

Volume average is carried out by averaging properties at an instant in time over a volume and ascribing the average value to a point in the flow. The volume-averaged conservation equations for the continuous phase (Eulerian framework) are given by:

$$\frac{\partial}{\partial t}\rho + \nabla\cdot(\rho\mathbf{u}) = -\frac{1}{V}\sum_k \dot{m}_k = s_{mass} \tag{1}$$

$$\frac{\partial}{\partial t}(\rho\mathbf{u}) + \nabla\cdot(\rho\mathbf{u}\otimes\mathbf{u}) = -\nabla p + \nabla\cdot\left(\boldsymbol{\tau}+\boldsymbol{\tau}^R\right) + \rho\mathbf{g} + S_{mom,ev} + S_{drag} \tag{2}$$

$$\frac{\partial}{\partial t}(\rho i) + \nabla\cdot(\rho\mathbf{u}i) = -p\nabla\cdot\mathbf{u} + S_{en,ev} + S_{conv} \tag{3}$$

$$\frac{\partial}{\partial t}(\rho\omega_A) + \nabla\cdot(\rho\omega_A\,\mathbf{u}) = \omega_{A,s,k}\, s_{mass} \tag{4}$$

where the stress tensor is:

$$\boldsymbol{\tau} = \mu\left(\nabla\mathbf{u} + (\nabla\mathbf{u})^T\right) - \frac{2}{3}\mu\nabla\cdot\mathbf{u} \tag{5}$$

The Reynolds stress tensor, $\boldsymbol{\tau}^R$, is modelled with the Boussinesq hypothesis and a two-equation model (k-ε realizable).

$$\boldsymbol{\tau}^R = -\frac{2}{3}(\rho k + \mu_t\nabla\cdot\mathbf{u})\mathbf{I} + \mu_t\left(\nabla\mathbf{u} + (\nabla\mathbf{u})^T\right) \tag{6}$$

Turbulent kinetic energy and dissipation rate are affected by the presence of the dispersed phase. This is known as *turbulence modulation*. However this modulation is weak if the particle concentration is low, as in OST two-phase flows. Therefore it has not been considered.

The source term of equation (1) represents mass exchange between phases due to droplet evaporation.

The source terms in equation (2) represent momentum exchange between phases due to droplets' evaporation, $S_{mom,ev}$, and momentum exchange due to surface forces (steady state drag force) at phases boundaries, S_{drag}:

$$S_{mom,ev} = -\frac{1}{V}\sum_k \mathbf{v}_k\dot{m}_k \tag{7}$$

$$S_{drag} = -\frac{3\pi\mu}{V}\sum_k d_k f_k\left(\mathbf{u}-\mathbf{v}_k\right) \tag{8}$$

The source terms of equation (3) represent energy exchange due to droplet evaporation, $S_{en,ev}$, and convective heat transfer between the phases, S_{conv}:

$$S_{en,ev} = -\frac{1}{V}\sum_k \dot{m}_k h_{s,k} \tag{9}$$

$$S_{conv} = \frac{\pi k}{V}\sum_k Nu_k d_k\left(T - T_{d,k}\right) \tag{10}$$

The source term in equation (4) represents mass exchange of species A between the phases due to evaporation.

The drag factor f is the ratio of the drag coefficient, C_D, to Stokes drag:

$$f = \frac{24C_D}{Re_r} \tag{11}$$

where the relative Reynolds number is:

$$Re_r = \frac{\rho|\mathbf{u}-\mathbf{v}|d_{drop}}{\mu} \tag{12}$$

The drag coefficient is evaluated with the Morsi-Alexander correlation [9] and is accurate over a wide range of Re_r:

$$C_D = a_1 + \frac{a_2}{Re} + \frac{a_3}{Re^2} \tag{13}$$

where a_1, a_2 and a_3 are constants that apply to smooth spherical particles.

LAGRANGIAN FRAMEWORK – SLURRY

The dispersed liquid phase is calculated with the Lagrangian approach by tracking a large number of *parcels* through the computational domain. A parcel represents a large number of real droplets with same properties, like velocity, temperature and diameter.

The droplet size distribution from each nozzle has been fitted to the data provided by the nozzles' supplier using the Rosin-Rammler expression. The complete range of sizes is divided into an adequate number of discrete intervals, each represented by a parcel, for which trajectory calculations are performed. The mass fraction of droplets of diameter greater than d is given by:

$$Y_d = e^{-\left(\frac{d_{drop}}{\delta}\right)^n} \tag{14}$$

where δ and n are two empirical constants, related to the measured droplets size distribution.

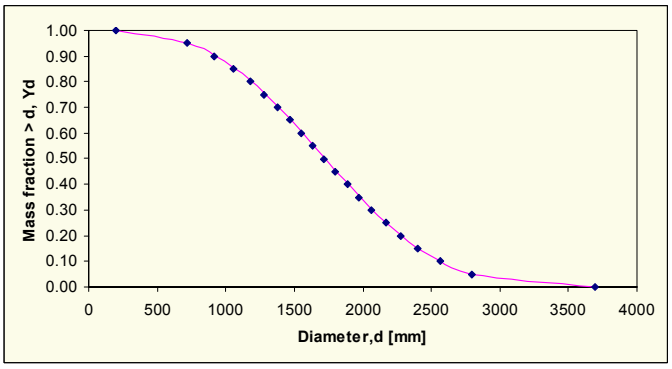

Figure 1 Rosin-Rammler correlation that fits the droplet size distribution provided by the nozzles' supplier

The equations of motion of each parcel are solved using the continuous phase flow properties at the current droplet position, and they have the following form:

$$\frac{d\mathbf{x}}{dt} = \mathbf{v} \tag{15}$$

$$\frac{dm_d}{dt} = \dot{m}_d = \frac{Sh \cdot D_{H_2O-air}}{d_{drop}}\left(\frac{P_{sat,H_2O}(T_d)}{\Re T_d} - \frac{n_i}{n}\frac{P}{\Re T}\right) \tag{16}$$

$$m_d \frac{d\mathbf{v}}{dt} = \mathbf{F}_{surf} + \mathbf{F}_{body} = \frac{1}{2}\rho C_D A\,|\mathbf{u}-\mathbf{v}|(\mathbf{u}-\mathbf{v}) + m_d\mathbf{g} \tag{17}$$

$$m_d c_d \frac{dT_d}{dt} = \dot{Q} + \dot{m}_d h_{lv} \tag{18}$$

Equation (17) assumes that the forces due to the flow pressure and shear stress gradient, the added mass force, the Basset force, the Magnus and Saffman forces are all negligible. The order of magnitude of these forces is the ratio between the gas and liquid density and therefore $O(10^{-3})$, which justifies the above assumption. The only surface force that appears in the droplet momentum equation is the steady-state drag force while the body force is gravity.

The droplet energy equation (18) is valid for Bi<0.1 and no radiative heat transfer. Only convective and latent heat transfer is considered.

$$\dot{Q} = Nu \cdot \pi \cdot k_c d_{drop}(T - T_d) \tag{19}$$

For spherical droplets, the Nusselt number, Nu, and the Sherwood number, Sh, are evaluated through the Ranz-Marshall correlation:

$$Nu = \frac{h \cdot d_{drop}}{k_c} = 2 + 0.6\,Re_r^{0.5}\,Pr^{0.33} \tag{20}$$

$$Sh = \frac{k_g \cdot d_{drop}}{D_{H_2O-air}} = 2 + 0.6\,Re_r^{0.5}\,Sc^{0.33} \tag{21}$$

where Re_r is the relative Reynolds number and Sc is the Schmidt number.

$$Sc = \frac{D_{H_2O-air}}{\nu} \tag{22}$$

The rate of H_2O mass transfer depends on the relative partial pressure between water vapour in the gas phase and the water vapour film surrounding the droplet, the latter evaluated through Antoine's law:

$$P_{H_2O,sat}(T_d) = e^{A-\frac{B}{T_d+C}} \tag{23}$$

Slurry density can increase due to droplet evaporation. The upper value is determined from the specified mass fraction of solids inside the reaction tank, which allows the calculation of the suspended solids volume fraction of every injected droplet.

$$\rho_d(t=0) \le \rho_d(t) \le \rho_s \tag{24}$$

Slurry viscosity has been supposed to have the same values as if it were water:

$$\mu_d(T_d) = \frac{\mu_0}{1 + 0.0337\,T_d + 0.00022\,T_d^2} \tag{25}$$

where $\mu_0 = 1.808 \cdot 10^{-3}\ {}^{kg}/_{ms}$ is the viscosity of water at 0°C and the temperature must be expressed in degrees Celsius.

DROPLET-WALL INTERACTION

A considerable amount of the injected slurry impacts on the scrubber internals, like walls and spray banks. Therefore it is necessary to handle the droplet trajectory modification due to this interaction.

Two different events can occur when a parcel hits a wall: splashing and deposition. Splashing occurs when the droplet impact energy exceeds an upper limit, i.e. when the droplet K-number, K_{drop}, exceeds a critical value, K_{cr}.

$$K_{drop} = Oh\,Re_l^{1.25} \tag{26}$$

where the wall-Reynolds number, Re_l, and the Ohnesorge number, Oh, are defined respectively:

$$Re_l = \frac{\rho_d |\mathbf{v}_{norm}| d_{drop}}{\mu_d} \quad (27)$$

$$Oh = \frac{We_l^{0.5}}{Re_l} = \frac{\rho_d |\mathbf{v}_{norm}|^2 d_{drop} / \sigma_d}{Re_l} \quad (28)$$

K_{cr} depends on surface characteristics such as surface roughness, surface curvature, wettability and film thickness. The present study has been done considering $K_{cr}=0$, that is complete rebound of every droplet impacting onto a solid surface inside the scrubber.

Figure 2 shows schematically a droplet impact onto a rigid stationary wall. The present work considers the empirical correlation of Weiss and Wieltsch [10], [11], that has been derived from experiments carried out with nozzles and wall materials commonly used in WFGD equipment. The velocity magnitude of the splashed droplets, $|\mathbf{v}_{reb}|$, and the ejection angle, β, from the wall film are respectively:

$$|\mathbf{v}_{reb}| = |\mathbf{v}_{imp}| - 0.04\alpha \quad (29)$$

$$\beta = 0.002\alpha^2 + 0.06\alpha + 8.1 \quad (30)$$

In equations (29) and (30) velocities are expressed in m/s and angles in degrees. The splashed droplets are assumed to be of same size and number as the impacting ones. Furthermore the tangential velocity component of a splashed droplet, $\mathbf{v}_{reb,tan}$, maintains the same direction as the impacting droplet tangential velocity component, $\mathbf{v}_{imp,tan}$.

SIMULATION AND RESULTS OF PILOT PLANT WFGD

A Pilot Plant counter current OST has been simulated and the numerical results have been compared with the available experimental data.

Table 1 summarizes the operating parameters of the equipment considered for the simulations and the main numerical settings.

Three different geometry discretizations have been analyzed. The number of injected droplets has been gradually increased, up to the value listed in Table 1, in order to achieve a solution independency from it.

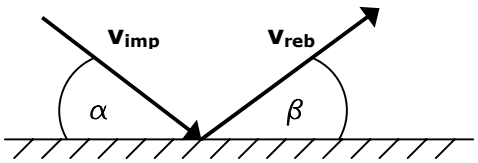

Figure 2 Schematic representation of a droplet impacting onto a solid surface

Spray zone	
Absorber Diameter	1.5 m
Height	8.3 m
Volume flow rate	13000 Nm³/h
Spray Banks	3
Slurry volume flow rate / level	96 m³/h
Nozzles	
Supplier	Spaying Systems
Nozzles / level	4
Volume flow rate / nozzle	24 m³/h
Spraying angle	120°
Type	Hollow cone Single flow
ΔP Nozzle	0.55 bar
Flue gas inlet temperature	160°C
Reaction tank	
Suspended solids content	15%wt.
Slurry density	1103 kg/m³
Slurry temperature	52.1°C
Numerical settings	
Coarse grid	
Number of control volume cells	700 000
Number of simulated parcels	36 000
Medium grid	
Number of control volume cells	1 577 094
Number of simulated parcels	36 000
Fine grid	
Number of control volume cells	3 392 167
Number of simulated parcels	36 000

Table 1 Main operating parameters and numerical settings of Pilot Plant scrubber

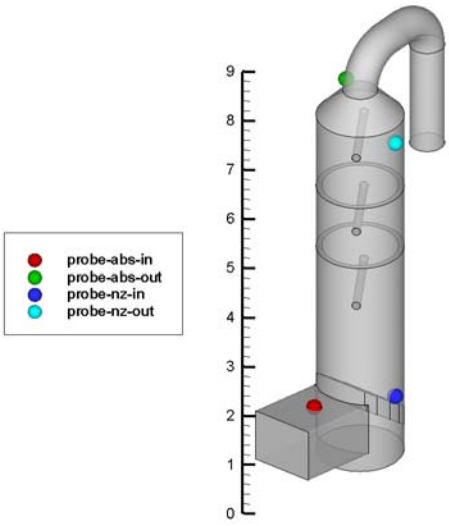

Figure 3 Pilot Plant geometry and position of the measuring probes

Figure 3 illustrates the geometry of the Pilot Plant WFGD unit with the measuring probes of pressure and temperature, while Figure 4 shows the domain geometry discretization with both tetrahedral (inlet and spray zone) and hexahedral (scrubber cone and outlet duct) finite volume elements.

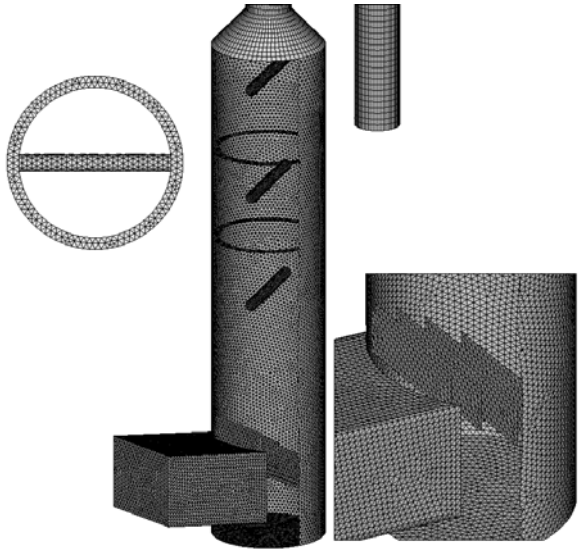

Figure 4 Geometry discretization with finite volumes; Tetrahedral and Hexahedral mesh elements

SIMULATION RESULTS

Figure 5 and 6 show calculated axial flue gas velocity for single-phase and two-phase flow operation, at two different positions along the scrubber.

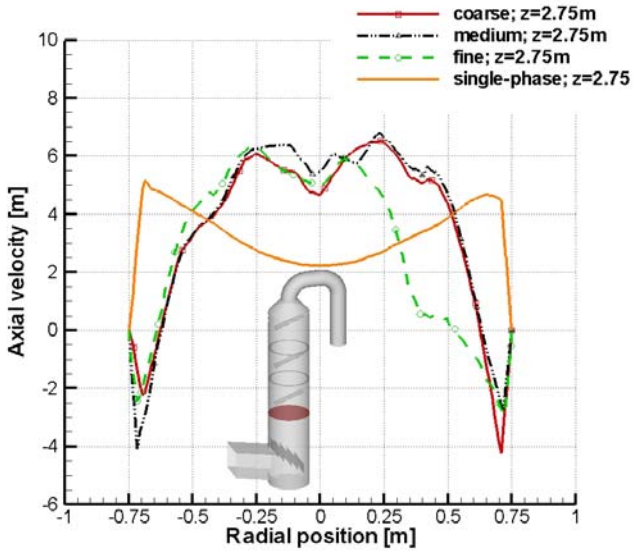

Figure 5 Calculated axial velocity profiles for single- and two-phase flow on a line located at z=2.75m, passing through scrubber center and directed normal to gas inlet

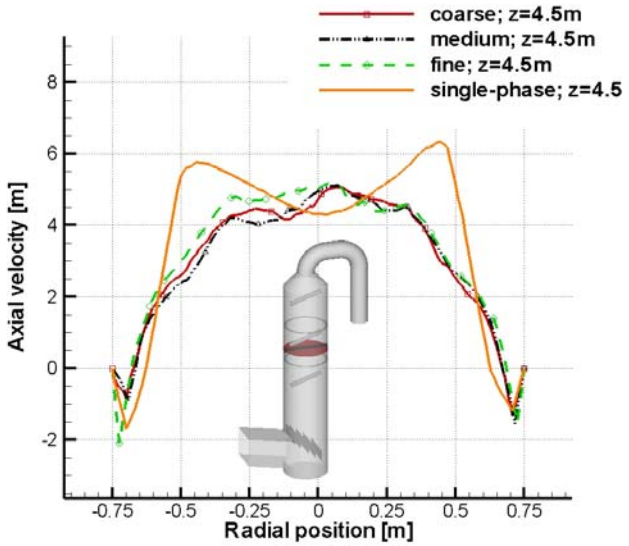

Figure 6 Calculated axial velocity profiles for single- and two-phase flow on a line located at z=4.5m, passing through scrubber center and directed normal to gas inlet

The liquid flow strongly modifies the single-phase velocity profiles. Hollow cone nozzles, with a wide opening angle of 120°, spray a substantial part of the injected liquid flow directly against the perimeter walls. This cause the formation of a wall liquid film, and the highest liquid volume fractions are thus located close to the walls. The flue gas tends to by-pass this dense spray region, where the velocity can be even directed downward, and is forced to move upward in the central region of the tower.

The three different geometry discretizations give quite similar results.

Figure 7 compares the calculated values of pressure drop, for the three different grids, with the experimental data. Figure 8 illustrates the comparison between the temperature values. The position of the probes is shown in Figure 3.

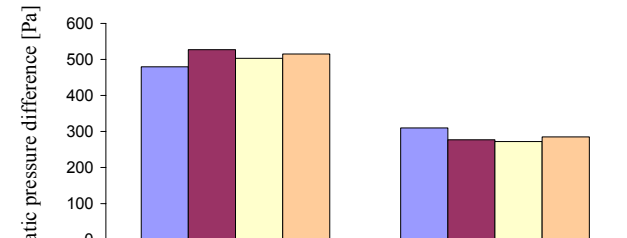

	Pilot Plant OST	Spray zone
exp	480	310
coarse	527.24	277.28
medium	503.46	272.44
fine	515.23	285.1

Figure 7 Comparison between calculated and experimental ΔP

$\Delta P_{\text{Pilot Plant OST}} = P_{\text{probe-abs-in}} - P_{\text{probe-abs-out}}$;

$\Delta P_{\text{Pilot Plant OST}} = P_{\text{probe-abs-in}} - P_{\text{probe-abs-out}}$

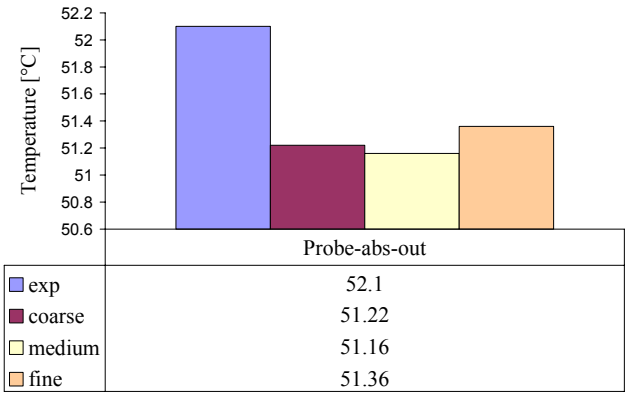

Figure 8 Comparison between calculated and experimental T

The simulation slightly over predicts the total OST pressure drop, while the spray zone pressure drop is slightly under predicted. The results seem to be quite independent from the mesh element number. The calculated temperature values are very close to the measured ones and the difference is less than 2%.

CONCLUSIONS

A two-phase flow of a Pilot Plant OST has been analyzed with a 3-D CFD model based on the Eulerian-Lagrangian approach. The numerical results are in good accordance with the experimental data, thus the local distribution of important process parameters, like slurry density and flue gas velocity, can be used to identify critical zones, which can be reduced in retrofits of existing OST or avoided in the design phase of new equipment. It can be concluded that CFD is a powerful tool in the design of counter current WFGD equipment.

Other simulations that account for partial slurry deposition on the walls have to be done and compared with experimental data.

The particle-wall interaction should be accurately investigated to find a suitable expression that can also include the possibility of a wall-film formation.

Furthermore, the physical presence of particles in the flow creates velocity disturbances that contribute to the Reynolds stress. Boussinesq assumption will not be valid because Reynolds stresses should be produced also in the absence of a mean velocity gradient. A better approach is the use of the Reynolds stress model (RSM) that avoids the use of the Boussinesq assumption.

REFERENCES

[1] Catalano G., LeRose R. and Lampropoulos L: State of the art wet FGD system for high sulphur fuels in Florina/Greece, Power-gen, Barcellona/Spain, May 25-27, 2004. 21 Pages

[2] Crowe C. T., Sommerfeld M., Tsuji Y., Multiphase flow with droplet and particles, *CRC Press*, 1998, pp.472

[3] Crowe C.T., Troutt T.R., Chung J.N., Numerical Models for two-phase turbulent flows. School of mechanical and materials Engineering, Washington State University, Pullman, Washington 99164 – 2920

[4] Crowe, C.T., Sharma, M.P., Stock D.E., The particle-source-in-cell (PSI-Cell) model for gas-droplet flows, *J. Fluid Eng*., 1999, pp.325-334

[5] Dudek S.A., Rogers J.A. and Gohara W.F.: Computational Fluid Dynamics (CFD) model for predicting two phase flow in a flue-gas desulfurization wet scrubber, *EPRI-DOE-EPA Combined Utility Air Pollutant Control Symposium*, August 16-20, 1999 Altanta, Georgia, USA. 6 pages

[6] Ferziger J.H., Peric M., Computational methods for fluid dynamics, *Springer*, Second edition, 1999, pp.389

[7] Ishii M., Hibiki T., Thermo-fluid dynamics of two-phase flow, *Springer*, 2006, pp.462

[8] Mundo C., Sommerfeld M., Tropea C., Numerical and experimental investigation of spray characteristics in the vicinity of a rigid wall, *Exp thermal Fluid Sci*, Vol 15, pp. 228-237

[9] Morsi S.A., Alexander A.J., An Investigation of Particle Trajectories in Two-Phase Flow Systems, *J. Fluid Mech.*, 1972, Vol. 55(2), pp.193-208

[10] Weiss C., The liquid deposition fraction of sprays impinging vertical walls and flowing films, *Int. Journal of Multiphase Flow*, Vol 31, 2005, pp. 115-140

[11] Weiss C., Wieltsch U., Laser optical flow measurements and computational fluid dynamic calculation of spray tower hydrodynamics, *Chemical Engineering Research and design*, Vol 83, 2005, pp. 1-17

ACKNOWLEDGEMENTS

The numerical simulation of this work has been performed on a Pilot Plant of ALSTOM. ALSTOM has also provided the necessary drawings of the plant and all experimental data.